Modeling of the Transformation Kinetics of Small Metal Particles during Combustion inside the Chamber of Hybrid Rocket Engines

Ognjan Božić[1], Noushin Mokhtari Molk Abadi[2], Georg Poppe[3] and Stefan May[4]
German Aerospace Center (DLR), Institute of Aerodynamics and Flow Technology (AS), Lilienthalplatz 7, D-38108 Braunschweig, Germany
[1]ognjan.bozic@dlr.de, [2]noushin.mokhtarimolkabadi@dlr.de [3]georg.poppe@dlr.de
[4] stefan.may@dlr.de

Abstract

Metal powders as fuel ingredients of hybrid rocket motors are an important factor which can improve the engine properties. Through the fuel density increase, a compact engine form can be achieved and the construction mass ratio can be reduced. Furthermore, the addition of metal powders in the fuel structure can increase the regression rate, the combustion temperature and the corresponding specific impulse. But to achieve these goals, the combustion efficiency of metal particles must be high and the condensation of metal droplets, high particle agglomeration, the combustor wall slagging as well as the nozzle structure abrasion must be reduced or completely avoided. The challenging experiments with hybrid rocket engines (HRE) deliver a limited amount of information necessary to understand transformation mechanisms, despite of the application of sophisticated measurement techniques. So, the experiments should be combined with CFD multiphase simulations to enable understanding of combustion processes related to the condensed flow phase. Subsequently, this enables the management of the combustion process within HRE as well as the avoidance of negative effects by the application of powder ingredients with metal content.
Within the AHRES (Advanced Hybrid Rocket Engine Simulation) program, the DLR Institute of Aerodynamics and Flow Technology in Braunschweig has carried out experiments with different fuel formulations, which included metal powders of aluminum and aluminum-magnesium alloys. Additionally, the transformation loop of small particles with metal content is simulated using an Euler-Lagrange coupling of the reacting gas flow and the condensed metallic phase. The conducted simulation includes time dependent transformations of Al and AlH_3 particles (decomposition, melting, vaporization, heterogeneous combustion, condensation and solidification). In this paper, the used transformation models and the coupling procedure between the gas and the condensed phase are classified and explained. For given start and boundary conditions one simulation of the characteristic small single metal particles with corresponding trajectories is realized. The results are graphically displayed and extensively commented. They enable helpful conclusions about the utilization of metal particles as fuel ingredients for HRE.

Keywords: hybrid rocket engine, CFD simulations, multi-phase flow combustion, condensed phase, metal particle kinetic

1. Introduction

Metalliferous small particles are used as fuel additives in hybrid rocket engines, as they promise an increase in performance in terms of specific impulse, regression rate, combustion temperature and the compactness of the fuel grain (and indirectly the combustion chamber too). They are added to the fuel as a powder of micro or nanometer sized particles. The additives can either be pure metals, metal alloys or metal hydrides. By exposure to heat, the metal hydrides release pure hydrogen, which can be then used for the combustion. But the use of these metalliferous particles also introduces problems into the combustion process, such as the appearance of the condensed phase (process still unexplored), the particle agglomeration and deposition on the chamber walls and increased nozzle erosion. To-date the worldwide conducted experimental studies related to this topic collected only limited information regarding the kinetics of the conversion of metalliferous small particles. In this work one approach to determine the kinetics of the conversion of metal particles by means of mathematical models has been developed. The applied mathematical models for the discrete phase (Lagrange approach) were coupled with an already existing

Euler model which describes the continuous flow and combustion in the gas phase without consideration the combustion of gasified metal. The impact of the combustion of metal particles on the gas flow phase has been taken into account through the correction of the local gas flow temperature, which corresponds to the contribution of released heat from gasified aluminium on the temporary particle position. The aluminium combustion is taken as most representative case, because it is frequently used in large fractions and has a very high reaction enthalpy. For details please see the Chapter 4.

2. Combustion of Metal Particles of HRE

2.1 Combustion of Al-Particles

The combustion process of metal particles can be well illustrated with the example of an aluminum particle (disperse phase) in the environment of gaseous combustion products (continuous phase).

As initial assumption the small aluminum particles are mixed in the polymeric binder structure during fuel grain production. For the present simulation it is assumed that the metal powder distribution in the grain structure is homogeneous. Once the hot oxidizer gas is injected into the combustion chamber it meets the fuel and ignites. At the same time a pyrolysis reaction on the fuel reacting surface occurs and the fuel binder begins to decompose. The solid aluminum particles contained in the fuel block are mixed homogeneously in the grain and begin to oxidize through the combustion process. The aluminum particles now heat up promptly and melt as soon as they reach a temperature of T_{par} = 933 K. Around the aluminum particles an oxide layer of Al_2O_3 is built, with a much higher melting temperature than the aluminum itself. The surrounding oxide layer of the aluminum particles breaks up due to the expansion of the liquid aluminum within the droplet. Through surface tensions the liquid aluminum flows out to the gas contact surface and can coalesce with other aluminum particles which cross the droplet's trajectory. Through this mechanism agglomerates with a particle size of 100-200 microns could be formed. Detached aluminum particles with a size of 5-40 microns are smaller than agglomerates.

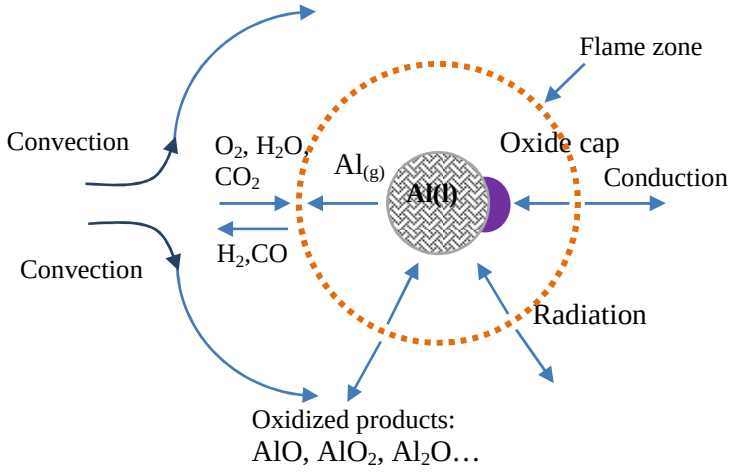

Figure 1: Schematic of the gas phase combustion of an aluminum particle in the combustion chamber of a hybrid rocket engine [22]

Agglomerates and detached particles do not burn in the same environment. Detached droplets burn close to the surface (due to their small size) in an oxidizer rich environment; agglomerates burns further from the surface, in an gas environment with lower oxidizer content because the oxidizer was partly used for the smaller droplets [6]. For HRE this mechanism cannot be taken as general valid, as by solid rocket motors, because the local oxidizer concentration depends on the injection scheme of the oxidizer into the combustor. By breaking up the oxide layer during the agglomeration (clustering process) the rate of particle oxidation increases, resulting in a rapid rise in temperature. Now the oxide layer melts if a temperature of T_{Al2O3} = 2327 K is achieved. Also through the breaking up of the aluminium oxide layer some oxide pico-particles could be expelled from droplet surface into environment building up a smoke zone around the particles.

Due to the high surface tension of the oxide surface and lower area of surface tension between oxide and metal, the liquid oxide layer (see Figure 1) pulls back and builds up accumulations which lie ahead of the aluminums droplets. Ignition takes place at the melting temperature of the aluminum oxide (Al_2O_3) at temperature T_{Al2O3} of 2327 K. The accumulation process (overcrowding) and the ignition are difficult to distinguish from each of other and are carried out in the same process step [6]. The combustion takes place between the melting temperature of the oxide layer and the evaporation temperature of the aluminum $T_{par, evap}$ = 2743 K. If the boiling temperature of aluminum is reached, it

begins to evaporate. However, the already existing accumulated oxide on the surface of the droplet decreases the evaporation rate of aluminum, because it covers a significant area of the droplet. In addition to a non-symmetrical combustion, a very rapid rotation of the droplet occurs. Finally, this rotation may also result in an enlargement of the droplet curvature due to change in surface tensions, diffusion, convection and heterogeneous reactions [6] while:

- As long as a certain area of the droplet is covered with the oxide cap, less gaseous aluminum can diffuse from the droplets into gas environment, then the oxide products such as AlO, Al_2O and AlO_2 diffuse into the droplets. Thus, these products condense on the relatively "cold" droplet surface.

- In addition, the formed alumina smokes (Al_2O_3) partly land on the surface of the droplet through convection and thermophoresis.

- Alumina (Al_2O_3) can be formed during a heterogeneous reaction between the liquid aluminum and the gaseous oxides, which surround the droplets, thus increasing the existing oxide cap. Since the boiling temperature of the alumina is not reached on the surface of the aluminums droplet, this reaction product remains after the aluminums consumption as residue [6].

In reality despite the reduced free droplet surface through the presence of an alumina cap a large part of the aluminums droplet evaporates. The gaseous aluminum reacts in a homogeneous reaction with the surrounding flue gas products (O_2, H_2O and CO_2). At the certain distance from droplet surface a freestanding, luminous flame front is formed with a size being 2- 4 times the diameter of the droplet. This combustion reaction generates the oxidized products AlO, Al_2O and AlO_2 where AlO represents the most common product. However, the oxidized products do not remain in the gas phase, because there is not enough heat available. They condense after leaving the flame and transform to Al_2O_3 smoke (clouds of pico- and nano- Al_2O_3 particles). Al_2O_3 smoke can also be formed through condensation of gaseous Al_2O_3. To start this condensation mechanism the evaporation temperature of alumina $T_{Al2O3,evap}$ = 3800 K must be first achieved, but it is possible only locally in the combustion chamber zones with free oxygen. The temperature of the gas cloud formation theoretically corresponds to the evaporation temperature of the alumina. The surface temperature of the droplet is also affected by radiation and conduction. How fast and how far a particle burns will depend on the conditions in the combustion chamber. The combustion process is complete once all of the aluminum has reacted. More details about combustion mechanism of aluminums particles can be found in the references [6], [7], [10], [19].

2.2 Combustion of Metal Hydride Particles

The transformation of other metal and metal hydride particles follows principally a similar logic as the transformation of aluminium particles within combustor.

Table 1: Physical and thermodynamic properties of the metals [3], [4], [2], [10], [27]

Metall	Symbol	ρ	c_p^0	T_{melt}	T_{boil}	M	H_{melt}	H_{boil}
		$[kg/m^3]$	$[kJ/K \cdot mol]$	[K]	[K]	[g/mol]	[kJ/mol]	[kJ/mol]
Aluminium	Al	2700	24,209	933	2743	26,98	10,7	293,0
Magnesium	Mg	1738	24,869	923	1363	24,3	8,7	128,0
Lithium	Li	535	24,623	453,69	1615	6,94	3,0	147,1

In Table 1 the ρ represents density, T_{boil} is boiling temperature, H_{boil} the boiling enthalpy and M is the molecular mass.

In this subchapter only the essential differences between the combustion of the particles of aluminium-magnesium alloys, alane and other metal hydrides particles with regard to combustion temperature, phase transformation temperatures (melting, evaporation, condensation, solidification, crystallisation) and decomposition mechanisms are compared.

Table 2: Physical and thermodynamic properties of metal hydrides, references [3], [4], [12], [15], [16], [17]

Name	Chemical formula	ρ [kg/m^3]	c_p^0 [kJ/K · mol]	T_{melt} [K]	T_{decom} [K]	M [g/mol]	H-content [% wt]	H_f^0 [kJ/mol]
Aluminiumhydrid	α-AlH_3	1477	40,235	-	373	30,01	10,1	-46,0
Magnesiumhydrid	MgH_2	1450	35,334	-	553	26,321	7,66	-76,1
Lithiumhydrid	LiH	775	27,957	961	1123	7,95	12,68	-90,7

In the Table 2 the T_{decom} is decomposition temperature; c_p^0 the specific heat by constant pressure and H_f^0 is enthalpy of formation.

3. Mathematical Model for the Determination of Aluminium Transformation Kinetics

3.1 General remarks

In this section the conversion kinetics of metal particles through chemical reactions are described with support of mathematical models. The goal is to demonstrate changes in the concentrations of the involved substances as a function of time.

Table 3: Overview of the different reaction orders

Reaction order	Example reaction	Reaction velocity	Unit	Example
0. Order	A ⟶ B	$v = k$	$\frac{mol}{m^3 \cdot s}$	Catalytic reaction
1. Order	A ⟶ B+C	$v = k \cdot \tilde{A}$	$\frac{1}{s}$	Decomposition reaction
2. Order	A+B ⟶ C	$v = k \cdot \tilde{A} \cdot \tilde{B}$	$\frac{m^3}{mol \cdot s}$	Combustion
3. Order	A+B+C ⟶ D	$v = k \cdot \tilde{A} \cdot \tilde{B} \cdot \tilde{C}$	$\frac{m^6}{mol^2 \cdot s}$	Collision reaction

Any chemical reaction takes place at a certain speed, called the reaction velocity. This indicates how many particles are converted from educt(s) to product(s) per time and volume unit. This value is calculated using the reaction rate and the concentrations of the involved reactants (s. Table 3). Generally, the reaction rate is determined by the Arrhenius equation:

$$k = A \cdot e^{\left(-\frac{E_a}{R_u \cdot T}\right)} \tag{1}$$

Here, R_u represents the universal gas constant, T is the reaction temperature, E_a the specific activation energy, and A a pre-exponential factor.

The concentration is an important parameter for the evaluation of the reaction rate, because the more reactant particles a volume contains, the more collisions occur statistically. Hence the reaction rate is increased. A reaction order can be found for any reaction, representing the number of reactant concentrations the reaction speed depends on. They are listed in Table 3 for various reactions. It should be noted that the different units for the reaction rate result from the various reaction levels.

Extremely fast reactions can be described using the concept of chemical equilibrium. The chemical equilibrium is a state in which the overall reaction appears dormant, so no changes are visible. The outwardly observable reaction rate is zero. Nevertheless, the chemical reactions (forward and backward reaction) continue to run with the same reaction rate. It is therefore not a static equilibrium, which it appears to be when examined externally, but a dynamic equilibrium in which reactions still proceed. In this state the Gibbs free energy for reacting compounds has its minimum and a general chemical equation can be given in the form:

$$a \cdot A + b \cdot B \leftrightarrow c \cdot C + d \cdot D \tag{2}$$

Here, a, b, c and d are the stoichiometric coefficients of the substances A, B, C and D. The equilibrium constant K_c results from the law of mass action which can be specified as a function of the concentrations of the involved substances as follows [2]:

$$K_c = \frac{[C]^c \cdot [D]^d}{[A]^a \cdot [B]^b} \tag{3}$$

The mentioned equilibrium constant is temperature dependent due to different concentrations of reactants and products at different temperatures. If the equilibrium constant is very large, the equilibrium is on the side of the products and there is a large fraction of products in the mix. Thus, almost all educts have reacted to products. If the equilibrium constant is very small, the equilibrium lies on the side of the educts, their fraction being accordingly large. For very rapid reactions it can be assumed that the chemical equilibrium is established instantaneously. In this case the non-equilibrium kinetic can be neglected.

3.2 Transformation Kinetics of Aluminium Particles

Within the combustion chamber of a hybrid rocket engine an aluminum particle passes through several conversion processes such as melting, evaporation, condensation and solidification into the glass or crystal phase.

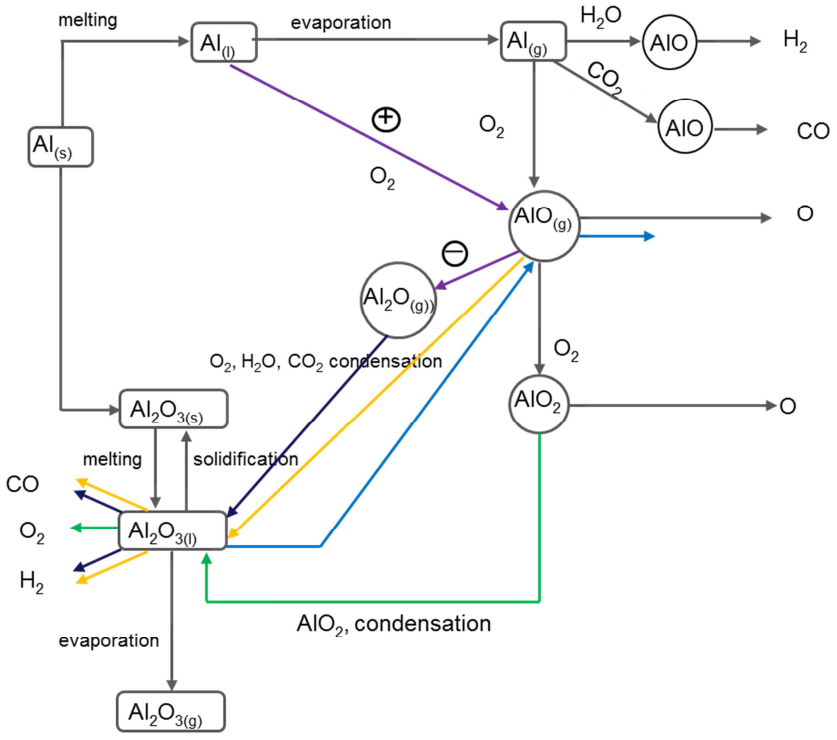

Figure 2: Schematic representation of the aluminium transformation and reaction in the combustion chamber of a hybrid rocket engine

Supplementary, the chemical reactions of aluminium with combustion products in gas phase occur parallel or sequentially. In Figure 2, the conversion and reaction processes of an aluminum particle during its combustion are shown schematically. The occurring chemical reactions can be grouped [22] as follows:

Surface reactions:

$$Al_{(l)} \longrightarrow Al_{(g)} \tag{R1}$$

$$Al_{(l)} + AlO_{(g)} \longrightarrow Al_2O_{(g)} \tag{R2}$$

Gas phase reactions:

$$Al_{(g)} + O_2 \xrightarrow{k_1} AlO + O \tag{R3}$$

$$k_1 = 9{,}76 \cdot 10^{13} e^{\left(\frac{-80}{T}\right)} \quad \text{in cm}^3\text{/mol s}$$

$$AlO_{(g)} + O_2 \xrightarrow{k_2} AlO_2 + O \tag{R4}$$

$$k_2 = 4{,}63 \cdot 10^{13} e^{\left(\frac{-10008}{T}\right)} \quad \text{in cm}^3\text{/mol s}$$

$$Al_{(g)} + CO_2 \xrightarrow{k_3} AlO + CO \tag{R5}$$

$$k_3 = 2{,}5 \cdot 10^{-13} T^{0{,}5} e^{\left(\frac{-1030}{T}\right)} + 1{,}4 \cdot 10^{-9} T^{0{,}5} e^{\left(\frac{14000}{T}\right)} \text{ in cm}^3\text{/mol s}$$

$$Al_{(g)} + H_2O \xrightarrow{k_4} AlO + H_2 \tag{R6}$$

$$k_4 = (1{,}9 \mp 1{,}5) \cdot 10^{-12} e^{\left(\frac{-442{,}87 \mp 221{,}44}{T}\right)} + (1{,}6 \mp 0{,}7) \cdot 10^{-10} e^{\left(\frac{-2868{,}6 \mp 452{,}94}{T}\right)}$$

Dissociation reaction:

$$Al_2O_{3\,(l)} \longrightarrow 2AlO + \frac{1}{2} O_2 \tag{R7}$$

Condensation:

$$2AlO + \frac{1}{2} O_2 \longrightarrow Al_2O_{3\,(l)} \tag{R8}$$

$$2AlO + CO_2 \longrightarrow Al_2O_{3\,(l)} + CO \tag{R9}$$

$$2AlO + H_2O \longrightarrow Al_2O_{3\,(l)} + H_2 \tag{R10}$$

$$Al_2O + O_2 \longrightarrow Al_2O_{3\,(l)} \tag{R11}$$

$$Al_2O + 2CO_2 \longrightarrow Al_2O_{3\,(l)} + 2CO \tag{R12}$$

$$Al_2O + 2H_2O \longrightarrow Al_2O_{3\,(l)} + 2H_2 \tag{R13}$$

$$AlO_2 + AlO_2 \longrightarrow Al_2O_{3\,(l)} + \frac{1}{2} O_2 \tag{R14}$$

The reactions R1 and R2 are surface reactions. The first reaction R1 is the evaporation of the melted aluminum. For small particles the transformation of R1 is so fast that it can be approximated as equilibrium process with sufficient accuracy (s. chapters 3.3 and 5.1). The second reaction R2 is assumed to be kinetically controlled for the small particles (less than 10µm) as suggested from Gremyachkin [30]. For small aluminum particles R2 is so fast, that the formation of Al_2O can be taken as infinite and is therefore neglected. With equations R3 - R6, the gas phase reactions of aluminium (homogeneous reactions) are described. The corresponding reaction rates given by [22] are shown. For the dissociation reaction of liquid aluminium oxide R7 it is assumed that only the dissociation temperature is responsible for the process devolution. This temperature is a function of the total pressure in the chamber, as well as the partial pressure of the aluminium sub-oxides and aluminium oxides. It reaches its maximum value as the droplet

passes through the flame zone. This maximum corresponds with the flame temperature. Reactions R8 - R14 describe the condensation of gasified aluminium sub-oxides into liquid Al_2O_3. This process involves two steps; homogeneous gas phase reactions, followed by homogeneous condensation. Since the reaction rate of the gas phase reaction is very high, its kinetics is neglected and the equilibrium state is assumed. The second step in which the homogeneous condensation takes place, the kinetics are described with the model in following subchapter 3.3.

3.3 Modelling of Phase Changes of Metal Ingredients (Melting, Vaporisation, Condensation and Solidification)

To calculate the mass fraction of the melted phase during the *melting* of the particle the following formula is applied [25]:

$$\frac{dX_{melt}}{d\tau} = \frac{1}{m_{par,0}} \cdot \frac{\dot{Q}_{kon}+\dot{Q}_{rad}+\dot{S}_{chem}}{\Delta h_{melt}} \tag{4}$$

Here $\dot{S}_{chem}$ is the heat of chemical reactions that could generally take place simultaneously with the melting process. This case is not considered in this work, because for analyzed ingredients parallel to melting no heat is generated by chemical reactions. The enthalpy of melting is denoted by Δh_{melt}. The melting fraction X_{melt} of a particle is determined for each time step. Since as fuel component applied metal particles are very small (diameters on the range of 0.0001-0.0030 mm), it seems likely that the particles melt abruptly. Before the melting temperature of the particles is reached (for aluminium is $T_{par,\ melt}$ = 933K) the melting fraction X_{melt} is 0. The maximum value for the melting fraction, which is equivalent to a complete melted particle (droplet), is X_{melt} =1.0. For the determined test case, computed under real combustor state condition, one aluminum particle with diameter of 5 µm is completely melted within 0,06µs. In consequence, the simplification that particle completely melts immediately and is dependent of its melting temperature, can be introduced. This process is also to refer as equilibrium process. However, for particles with higher diameters should be proved whether the melting process is to consider as time dependent and as non-equilibrium.

The modeling of the *evaporation* is to calculate, similar to upper given equation (4), in the form:

$$\frac{dX_{evap}}{d\tau} = \frac{1}{m_{par,0}} \cdot \frac{\dot{Q}_{con}+\dot{Q}_{rad}+\dot{S}_{chem}}{\Delta h_{evap}} \tag{5}$$

In expression (5), instead of melting enthalpy, the enthalpy of vaporization is in the denominator incorporated. Additionally, for the applied metal ingredients during analysed evaporation processes no heat of chemical reactions is generated, therefore $\dot{S}_{chem}$ = 0 can be assumed. The evaporation occurs when the evaporation temperature of the droplet is achieved. For an aluminium droplet this temperature is T_{evap} = 2743 K. The droplet is completely evaporated when evaporation fraction is X_{evap}= 1 and droplet mass vanishes. In the simulation presented here (for details see Chapter 5) the Al droplet starts to evaporate at 2,992 ms and is fully evaporated at 2,999 ms. That means that a droplet with an initial diameter of 5µm is completely evaporated after 7,0µs. In such case the process can be considered as instantaneous and depends only on the temperature level. For droplets with larger diameter, with evaporation time in the vicinity of 1ms this simplification does not apply.

Condensation - the resulting combustion products sub-oxides AlO, Al_2O and AlO_2, described with reaction equations R8-R14 (shown in section 3.2) are not preserved during the combustion process. They condense immediately from gas state to aluminum oxide Al_2O_3(l). Within the presented work it is tried to model this process as time dependent non-equilibrium process using the model of Beckstead [22], but a number of constants given in regression rate laws of the corresponding reactions unknown, making a calculation using the method unmanageable.
Here, the condensation from gas state is considered as process in equilibrium state toward Guldberg and Waage law [2] and tested on example of R8 [$2AlO + ½\ O_2 \rightarrow Al2O_{3\ (l)}$] equation using the NASA CEA2 code. For different temperatures and the constant chamber pressure of 43 bars the mass fraction of educts and products were determined with the CEA code [29]. From known mass fraction and prescribed temperature range the equilibrium constant is computed:

$$K_c = \frac{[Al_2O_3]}{[AlO]^2\,[O_2]^{0.5}} \tag{6}$$

The results are represented in Figure 3. The decrease of calculated constant K_c value is to observe at higher temperatures.

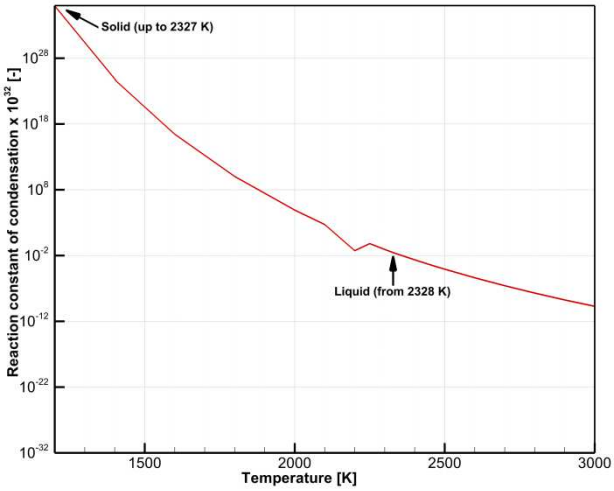

Figure 3: Equilibrium constant value K_c devolution over the temperature T for the reaction formula R8.

With the knowledge that by $K_c > 1$ the balance is on the side of products and by $K_c < 1$ is on the side of the reactants. This K_c value drop originates from the higher mass fraction of AlO at higher temperatures. Nevertheless, for $K_c > 1$, it can be concluded that this reaction proceeds with a very high proportion of Al_2O_3 as product. Due to this high value K_c it can be assumed that by temperature decrease the AlO is immediately and completely converted to Al_2O_3. Depending on the temperature level, the alumina is presented in the solid or liquid state.

Solidification refers to the phase transition from liquid to solid state. It is the reverse process to melting and usually occurs immediately once the melting temperature is underrun. For pure substances the melting temperature corresponds to the freezing temperature (begin of solidification). When alloys or mixtures of liquid are considered a phase diagram for determination of the freezing point must be taken into account. During solidification, whereby the thermal motion of the molecules decreases (Brownian motion) appears the crystallization. For the modeling of solidification with participation of crystallization in the reference [25] is given the JMAK- (Johnson-Mehl-Avrami-Kolmogorov) model. This model describes the nucleation and the growth of crystals within the particles. Thus different processes of crystallization, recrystallization and decomposition can be described with this model:

$$f(X) = n(1-X)[-\ln(1-X)]^{\frac{n-1}{n}} \qquad (0.5 < n < 4) \qquad (7)$$

The model describes the general solidification process very well. But the crystallization is usually a slow-running process, which take relatively long to complete (several seconds). With rapid cooling, where glass and no crystal is formed, this model does not apply. The rapid processes during droplet freezing/ solidification which appears within 1 ms or less are to model only as temperature dependent. In larger engines by temperature drop the characteristic temperature gradient is responsible whether the solid phase appears as glass or crystal. The aluminum particles don't solidify within the combustion chamber, since they have a relatively low freezing point, but it is quite realistic that some aluminum particles in the combustion chamber are not consumed and later in the nozzle where lower temperatures prevail, solidify. However, the substances created in the combustion chamber through chemical reactions by undershooting the own freezing temperature change in the solid phase. This process usually occurs at the end of the combustion chamber or in the "cold" combustion-chamber wall on. From the reaction formulas R1-R14 can be seen that only aluminum oxide (Al_2O_3) exists as a liquid product. The remaining compounds are in gaseous form and do not reach at the prevailing temperatures in the combustion chamber its freezing point. Al_2O_3 has a solidification temperature of T_{sol} = 2327K [28], therefore it can be assumed that at the end of the combustion chamber solid alumina is formed. Own experimental analyses have shown that alumina leaves the nozzle of a hybrid rocket in solid state.

3.4 Combustion of Gasified Aluminum under the Condition of Chemical Non-equilibrium

The reactions R3 – R6 mentioned in Chapter 3.2 are chemical reactions of second order (s. classification: Chapter 3.1 - Table 1). Once the mass reduction of aluminum particles through chemical reactions with the flue gas products in the chamber of HRE have been calculated, it does not make sense to only consider a single particle. The reason for this is the small size of the aluminum particles (d_{par} = 5 µm) and at the same time very fast chemical reactions. Therefore, in numerical calculations very small numbers are produced that are below the compiler accuracy, which was used to produce executable code. Therefore, a spherical gas cloud which consists of many aluminum particles and flue gas products is considered. In Figure 4 this concept is shown schematically. The sphere is set to a diameter of d_{cloud} = 1 mm. It can be assumed that this cloud moves along a selected stream line within the combustion chamber flow. The speed equates to the gas flow velocity along the stream line.

It is further assumed that all particles move in the gas cloud with the same velocity along a streamline. In order to show the change of the mass of involved substances over time, the mass fraction of these substances must be determined at each time step. The total mass of the gas cloud at the start point (fuel surface) corresponds to the sum of mass of flue gas products and the mass of aluminum particles.

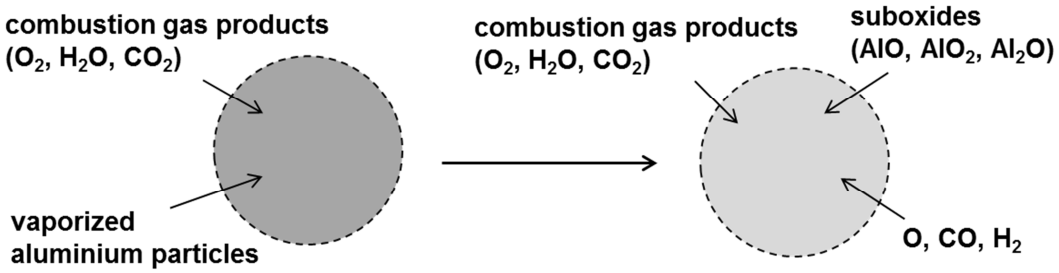

Figure 4. Cloud model for description of combustion of gassed aluminium

Further, the mass concentration of solid particles in the gas cloud on the start point is proportional to the fraction of metal ingredients in the solid fuel grain. Knowing the density of the gas phase mixture (input from CFD simulation) and aluminium particles density the relevant volume fractions of both phases can be calculated. The amount of particles n_{par} in the gas cloud can be calculated through

$$n_{par} = \frac{m_{Al,cloud}}{m_{Al}} \tag{8}$$

Here $m_{Al,cloud}$ is the total mass of aluminium particles in the cloud and m_{Al} is the mass of a single Al particle with known diameter. Hereby the initial conditions for the simulation of the Al particle transformation are defined.
The mass change of gas reaction educts and reaction products as a function of the time in equations system R3 - R6 can be described with a system of ordinary differential equations (ODE). The form of the mentioned ODE will be explained exemplary through the reaction $Al_{(g)} + O_2 \xrightarrow{k_1} AlO + O$ (R3):

$$\frac{d\, m_{Al,cloud}}{d\, \tau} = -\nu_{Al} \cdot V_{gas} \qquad \left[\frac{kg}{s}\right] \tag{9}$$

$$\frac{d\, m_{O2}}{d\, \tau} = -\nu_{O2} \cdot V_{gas} \qquad \left[\frac{kg}{s}\right] \tag{10}$$

$$\frac{d\, m_{AlO}}{d\, \tau} = \nu_{AlO} \cdot V_{gas} \qquad \left[\frac{kg}{s}\right] \tag{11}$$

$$\frac{d\, m_{O}}{d\, \tau} = \nu_{O} \cdot V_{gas} \qquad \left[\frac{kg}{s}\right] \tag{12}$$

Here V_{gas} is the gas volume of the particle cloud, v_{Al}, v_{O2}, v_{AlO} and v_O are the reaction rates [kg/$m^3_{gas} \cdot s$]. With the knowledge of the reaction rates, the mass change for each time step $d\tau$ can be determined. The shown principle was applied to R4 –R6. Through combination of all equations, a model for the chemical gas reactions was created.

The complexity of this model can be illustrated by considering some dependencies. For example, in equation R3, the concentration of AlO increases; in equation R4 this concentration decreases, because the AlO is an educts. In equations R5 and R6, the concentration of AlO increases again. In addition to this, the liquid phase reactions must be considered. This happens simultaneously and must be modeled accordingly. This interlaced dependence of referred reactions in this work was taken into account.

3.5 Transformation Kinetics of Alane

Alane AlH_3 comes in seven different crystalline phases (α, α', β, γ, δ, ε, ζ), whereof the structure of only three phases is known [11]. Most phases of alane dehydrogenate even at room temperature. That is the reason why they are not applicable as additives for fuel [10]. The most stable phase is α-AlH_3 which starts dehydrogenation at a temperature of about 373 K [4]. Alane does not have a liquid phase, as it is decomposed into aluminum and hydrogen. With the combustion begin only the dehydrogenation takes place, the hydrogen leaves the alane and pure aluminum remains as particle. The following reactions describe this process and the oxidation of the aluminum [12]:

$$AlH_3 \longrightarrow Al + 3/2\ H_2 \quad \text{(alane dehydration/ decomposition)} \tag{13}$$

$$Al + 3/4\ O_2 \longrightarrow 1/2\ Al_2O_3 \quad \text{(oxidation)} \tag{14}$$

Of essential importance for the modelling of decomposition of alane AlH_3 is the knowledge of the regression rate. Literature regarding this topic is unfortunately rare. But with a known decomposition time [10] the decomposition rate $\dot{r}_{dec}$ can be determined through a few mathematical operations.

$$\dot{r}_{dec} = \frac{V}{\tau_{dec}\, A} \tag{15}$$

In Equation (15) the value V is the particle volume, τ_{dec} is the experimentally estimated decomposition time and A the particle's surface. The composition of the gas mixture in particle's environment, especially partial pressure of O_2, CO, CO_2 and H_2O, has a significant influence on the decomposition time and has to be considered throughout the calculations.

4. Description of the Coupling Procedure Between the Discrete Phase and the Reacting Gas Flow

In this paper, the simulation model is shown, which describes the kinetics of the transformation processes in the discrete phase during the combustion of the metal or metal hydride particles in a hybrid rocket combustor. Since the particles are influenced by the dominating conditions of the gas phase within the combustion chamber, this simulation model was coupled with a model based on an Euler approach that describes the flow and combustion in

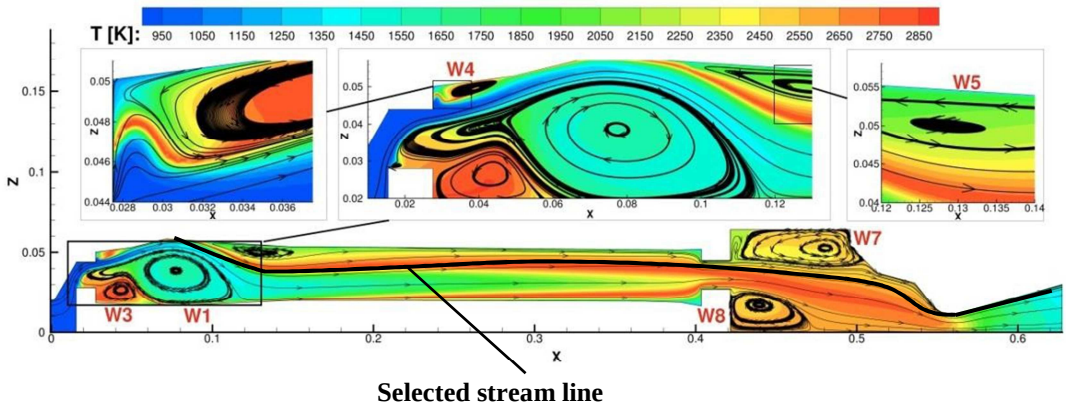

Figure 5: Temperature distribution and vortex formation of 2.5D simulation after 10 seconds burning time with the representation of the selected stream line (thick black line) [26].

the gas phase. In the work of S. May [26], the processes in the gas phase have been simulated with the TAU code. In the following subchapter, the coupling procedure between gas flow and discrete phase is described in more detail. Figure 5 shows the temperature distribution of a 2.5D simulation after a burning time of 10 seconds [26]. To investigate the transformation kinetics of the metal particles, in the present work one stream line has been selected. The metal flue gas cloud moves along this stream line (for details s. Chapter 3.5). The selected stream line does not touch the combustion chamber wall. In the frame of caried out 2.5D simulations of the gas flow the influence of combustion of gasified aluminum on the process was neglected. This procedure was eligible, because for metal particles/ droplets with diameter less than 5 µm the Stokes number is considerabelly lower than 1. In that case the observed particle follow the stream line of the gas phase, while the inertial force of the small particle are not dominant. The dominant influence is caused by the aerodynamic force on the particle. The particle's trajectory follows the selected stream line and for the computation of the particle's properties the gas temperature T_{gas}, the gas pressure p_{gas} and the gas velocity u_{gas} are applied.

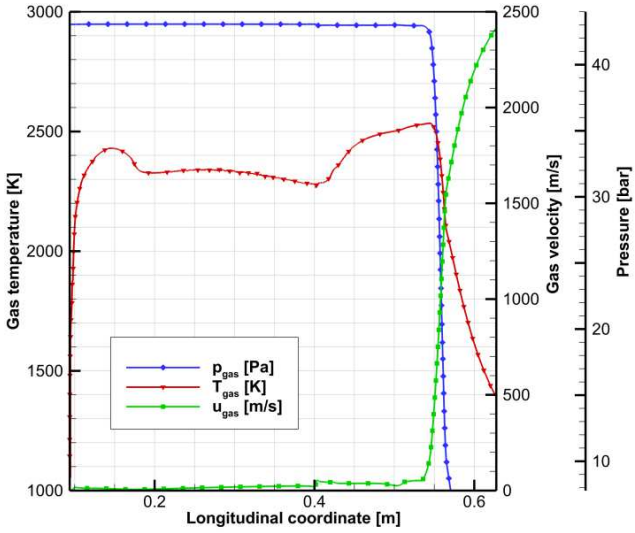

Figure 6: Progression of T_{gas}, p_{gas} and u_{gas} over the combustion chamber length along the selected flow line (the combustion of aluminum excluded) [26]

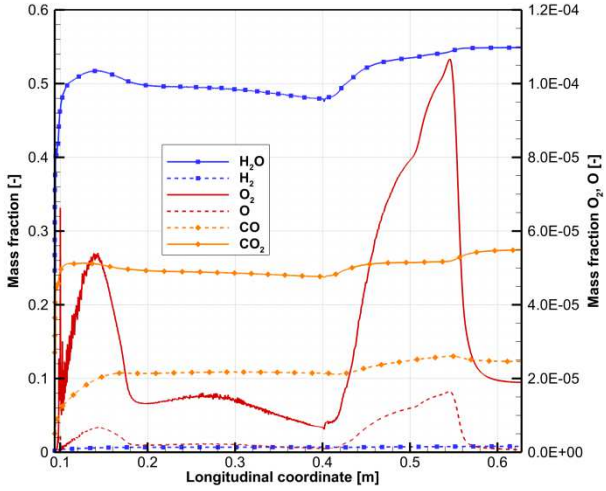

Figure 7: Progression of gas components H_2O, H_2, CO_2, CO, O_2 and O over the combustion chamber length along the selected flow line (calculated without combustion of aluminum) [26]

In the simulated case (see Figure 6) the gas temperature along the stream line at the beginning is T_{gas} = 1050 K (corresponding the pyprolysis temperature). Neglecting the combustion of aluminum particles, a maximum temperature of T_{gas} = 2550 K along the streamline can be achieved. Behind the combustion chamber at the nozzle outlet the temperature drops to a value of about 500 K. Along the stream line within the combustion chamber, of the pressure is approx. constant at p_{gas} = 43 bar. In the vicinity of the nozzle outlet this pressure drops and finally reaches the ambient pressure. The local velocity along the stream line inside the combustion chamber varies between 10 and 50 m/s; behind the chamber the velocity rises due to gas expansion inside the nozzle.

In Figure 7, the devolution of the stream line curve of the gas components H_2O, H_2, CO_2, CO, O_2 and O expressed as mass fractions are shown. The mass fractions of H_2 and O are very small compared to the mass of the remaining gases. The amount of H_2O and CO_2 along the selected stream line is very high, and they are most represented components among the combustion products. The mass fraction of the H_2O gas is in the range of 0.5 to 0.55; the CO_2 mass fraction varies from 0.24 to 0.28. Furthermore, a strong increase of the mass concentration of O_2 at a longitudinal coordinate between 0.4 – 0.55 m can be recognized. This results from the mixing the free oxygen molecules from the core flow and combustion products inside the secondary combustion chamber. The following data along the stream line are extracted from the gas phase flow simulation [26] data: x- and z-coordinates, velocities u_x and u_z in x- and z-direction, temperature of the gas flow T_{gas}, pressure of the gas flow p_{gas}, density of the gas flow ρ_{gas} and mass fraction of the gas components H_2O, H_2, O_2, O, CO, CO_2.

Using the above imported data, the distance and the travelling time of the particles until the outlet of the combustion chamber can be calculated with:

$$ds_{par} = \sqrt{(x_1 - x_0)^2 + (z_1 - z_0)^2} \tag{16}$$

The distance between two known points of the particle trajectory (which corresponds to the calculated streamline) is determined by the Euclidean approach for the distance calculation. The sum of all distances gives the total distance exposed by:

$$s_{par} = \sum_{i=1}^{n} ds_{par,i} \tag{17}$$

The flow time of the particle between two neighbor trajectory points (which coicide with defined points of stream line) can be determined by the following expression:

$$d\tau_{par} = \frac{dS_{par}}{u_{gas}} \tag{18}$$

Since the particles according the model assumption follow the stream line (Stokes number <<1), the local velocity is calculated at this point. The calculation of the particle motion is than to calculate as follows:

$$u_{gas} = \sqrt{u_x{}^2 + u_z{}^2} \tag{19}$$

The sum of all times increments gives the total traveltime of the particles in the combustion chamber:

$$\tau_{par} = \sum_{i=1}^{n} d\tau_{par,i} \tag{20}$$

The computation of the particle temperature T_{par} is done by applying the enegy balance equation for the particle

$$\frac{dT_{par}}{d\tau} \cdot m_{par,0} \cdot c_{p,par} = \dot{Q}_{con} + \dot{Q}_{rad} \tag{21}$$

From this equation also the heating rate can be determined. It is an important parameter needed for the identification the change of aggregation state of the metal particle/droplet. Here $m_{par,0}$ is the particle mass at the initial calculation step and $c_{p,par}$ is the specific heat capacity of the particle material. To calculate T_{par}, the gas temperature T_{gas} at any trajectory point along the selected stream line must be known and given as input for the simulation. To solve the ODE (21) which describes the energy balance and the current value T_{par} the Runge-Kutta-Fehlberg method of 4th order is applied. The convective heat transfer $\dot{Q}_{con}$ is given with folloving well known formulation:

$$\dot{Q}_{con} = h_\alpha \cdot A_p \cdot (T_{gas} - T_{par}) \tag{22}$$

The variable A_p is the particle surface and the h_α heat transfer coefficient to particle. The calculation of the heat transfer coefficient is done by considering the heat transfer to a sphere. In the literature [23] the following expression is favored:

$$h_\alpha = \frac{Nu\ k_w}{d_{par}} \tag{23}$$

Here, d_{Par} is the diameter of the particle, k_w is the thermal conductivity and the Nu the Nusselt number. For the Nusselt number the expressions Nu =2 can be used for very small Reynolds numbers [23]. For the computation of the radiation $\dot{Q}_{rad}$ the radiation model of [1] is applied. Based on past experience and theoretical analysis [24] the radiation flux can be assumed as 30 % for simple test calculations of the convective heat flux:

$$\dot{Q}_{rad} = 0{,}3 \cdot \dot{Q}_{con} \tag{24}$$

Since the influence of reacting aluminum particles on the combustion in the gas flow was not considered in the realized simulations [26], the maximum gas temperatures achieved in the combustion chamber are limited to 2550 K (analysed propellant combination HTP/HTPB). This temperature is below the evaporation temperature of aluminum, and therefore, no aluminium would take part in gas phase reactions. In reality, the gas temperature rises through the useage of aluminum particles as fuel additives, because the reaction of pure Al is exothermic. To obtain realistic results, the gas temperature was raised by aproximately 300 K. This value originates from the comparison of the gas temperatures which includes aluminium combustion and combustion without aluminum, determined using the NASA CEA2 code.

5. Evaluation of the CFD Simulation

The aluminum particle/gas cloud flies through the combustion chamber for about 30 ms on the flight length of approximately 0,525 m along the extracted stream line the environmental properties are known. In Chapter 4, a model for the temperature of the particle/droplet along its flight path is shown (s. equation 21). A strong dependence of the gas temperature on the particle temperature was expected.

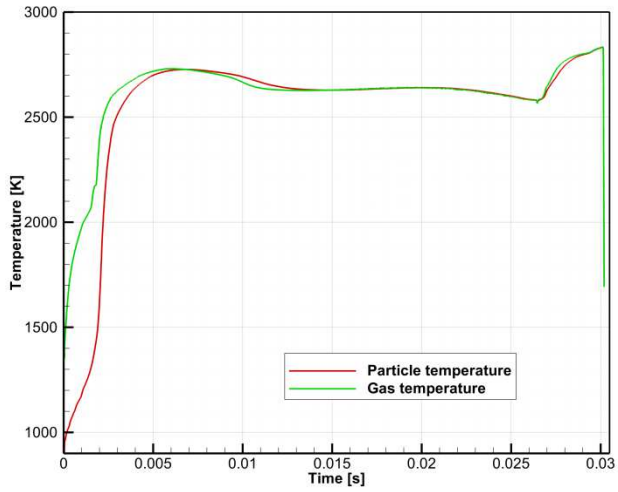

Figure 8: Modelled curves of the particle temperature T_{par} and gas temperature T_{gas} over the time [20].

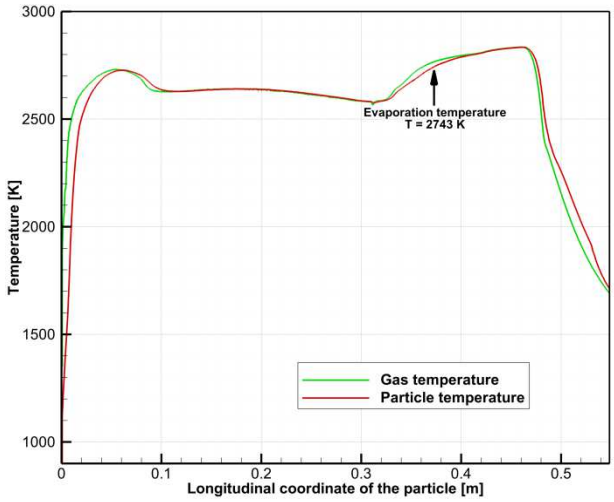

Figure 9: Modelled curves of the particle temperature T_{par} and Tgas temperature T_{gas} on longitudinal coordinate of the particle s_{par} by the combustion chamber [20].

In Figure 8, the modeled curves of the particle temperature and the gas temperature are plotted versus the time. At t = 0 s a particle temperature of T_{par} = 900 K was specified as the initial value. It is assumed that the particles temperature in the fuel block is below the gas temperature. Hence, at the beginning, the temperature difference of the gas and the particles is significant. The particles need approx. two millisecond to heat up. Gradually the particles temperature reaches the gas temperature. After about 15 ms from start point (release point from fuel) there is hardly any recognizable difference between particle temperature and gas temperature. In Figure 9 the particle temperature and gas temperature are plotted over the flight path of the particle for the same case. In this way, the heating of the particle can be clearly seen in the first few centimeters of the flight path. A very good approximation to the gas temperature is reached after approximatelly 0.1 m. In both, Figures 8 and 9, a drop in temperature is observed at the end of the trajectory. The reason is the shape of the convergent-divergent exhaust nozzle, which is connected to the end of the combustion chamber. Through the nozzle, the combustion products are expanded and cooled down.

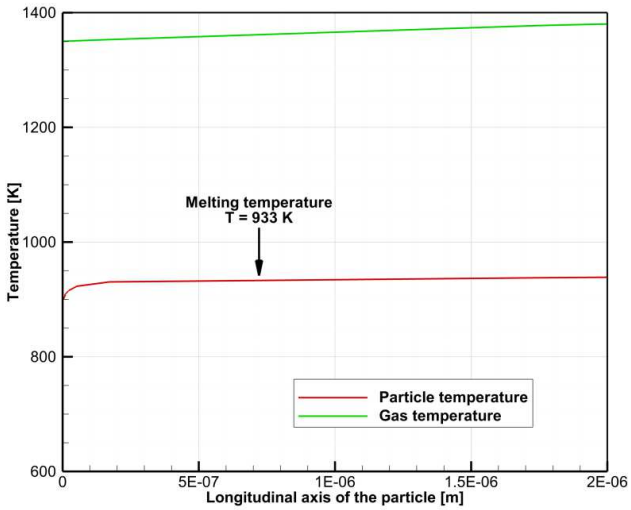

Figure 10: Enlarged view of the modeled curves of particle temperature and gas temperature on the longitudinal coordinate of the particle trajectory s_{par} with identification of the melting location

5.1 Melting and Evaporation

It was explained earlier (s. Chapter 3) that the melting and evaporation process of the aluminum particles is very fast. Therefore the respective process can be considered as instantaneous. No melting or evaporation fraction will be built. These phase transformations are exclusively dependent on the temperature, so it can be approximated that these processes are taking place under thermal equilibrium conditions. The phase transformation time intervals have been documented in Chapter 3.3. The melting of the particle occurs at 0.0008 mm from starting point and the evaporation of the Al droplet occurs at 0.37 m from starting point (see Figures 9 and 10).

5.2 Gas reactions without condensation

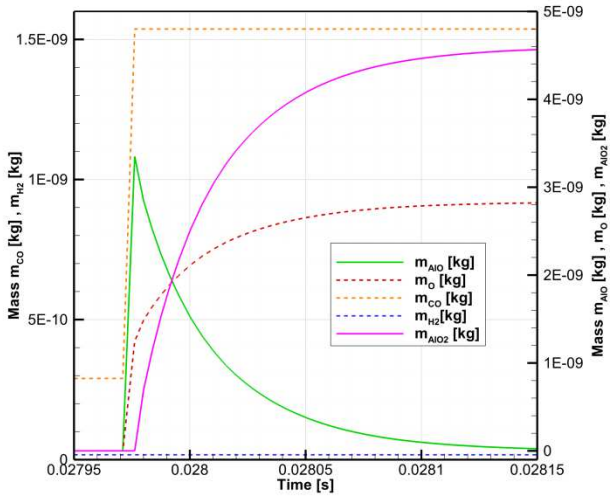

Figure 11: Modeled curves of the mass increase due to chemical reactions of various gas components in the gas cloud over the time [20]

Here the simulation results for gas-phase reactions based on Equations R3 - R6 are analyzed and displayed. The gas-phase reactions do not start until the evaporation temperature of the aluminum particle T_{evap} = 2743 K is reached. As soon as it is gaseous, it may react with the flue gas products. Due to the high reaction rate in equations R3 and R4 aluminum Al and oxygen O_2 undergo a very quick reaction to AlO, AlO_2 and O. The amount of water vapor H_2O and carbon dioxide CO_2 remains almost constant despite chemical reactions. This is due to the low reaction rates in the Equations R5 and R6. Figure 11 shows modeled curves of the mass change due to chemical reactions of various gas components in the gas cloud over time. It should be noted that AlO acts as a product in equations R3, R5 and R6, in equation R4 however, it is an educt. For this reason, the mass of AlO increases until the aluminum is completely consumed and decreases thereafter due to the much higher rate of reaction equation R4 compared to R5 and R6. It is also observed that the mass of CO and H_2 remains almost constant, although chemical reactions take place. The reason also lies in the low reaction rate of the equation R5 and R6.

5.3 Gas phase reactions with condensation

In Chapter 3.3 the solely virtual existence of AlO, Al_2O and AlO_2 was demonstrated by means of equilibrium constants in equations R8 - R14. Once they are formed, they oxidize in a chemical reaction with the flue gas products (O_2, CO_2 and H_2) and condense to liquid aluminum.

The result of the analysis of the condensation process is shown in Figure 12. The mass of AlO and AlO_2 is zero for the whole time because they react immediately to Al_2O_3 (l) as soon as they originate. The mass of Al_2O_3 (l) increases and reaches a constant value as soon as the aluminum is consumed completely. Later the liquid aluminum further transforms due to a decrease of temperature in the solid aluminum (s. next section - solidification).

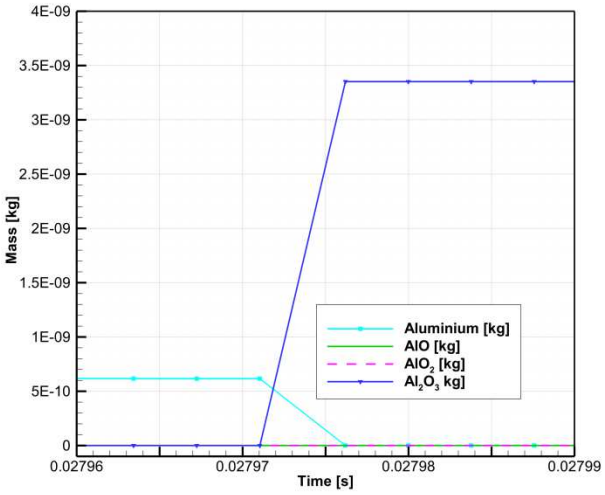

Figure 12: Modeled mass devolution over the time of involved constituents during the condensation process

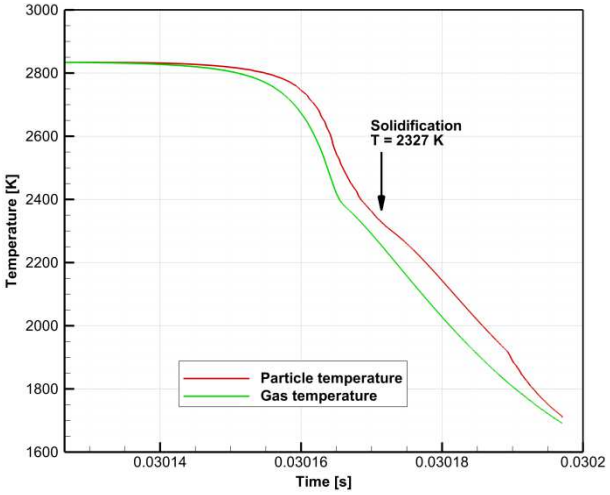

Figure 13: Enlarged view of the modeled curves of particle temperature and gas temperature over time with marking the solidification point.

5.4 Solidification of Liquid Aluminium

Liquid aluminum is the major product of the combustion of aluminum particles within a hybrid rocket engine. However, due to the temperature reduction it doesn't remain in the liquid state. In subchapter 3.3 it was shown that the solidification of aluminium oxide droplets can be considered as a function of temperature. After its formation the Al_2O_3 droplet will immediately change into the solid state at a temperature of T_{sol} = 2327 K . In Figure 13 the exact time of solidification point can be extracted at a distance of 0.487 m from start point. The aluminium oxide Al_2O_3 exits at the nozzle end as a solid particle (glas phase).

6. Conclusion

In this paper the transformation kinetics of aluminum particles within the combustion chamber of HRE has been studied in more detail. Aluminum particles compared to other metals have the best performance, since they achieve the highest specific impulse due to the high heat of oxidation and reaction enthalpy. Additionly, they have a high density, thereby providing a compact solid fuel grain form. This has a positiv influence on mass construction ratio of the whole rocket launcher. The mathematical models have been implemented in executable code and coupled with CFD code TAU, which simulate the combustion process within the HRE (Euler approach). With these models the transformation processes during melting, evaporation to gas state, condenstion from gas state, solidification, different types of diffusion prozesses, as well as chemical reactions of metal particles and their suboxides with the surrounding flue gas products have been successfully described. The investigated aluminum particles have a diameter of d = 5 microns; they move along the selected stream line within the combustion chamber without coming in contact with the chamber walls at any point. Along the streamline specially the motion and transformation of a multiphase gas/Al-particle cloud with a diameter of d = 1 mm were analysed. The kinetics of melting and the evaporation process were described with models which determined the melting or evaporation mass rate. Under the described conditions, the aluminum particle is melted within only 0,06 µs and evaporated within 7,0 µs. In that case the process can be described using the equilibrium state conditions. The chemical processes within the cloud have been regarded as non-equilibrium processes. The determination of the kinetics of chemical reactions between aluminum particles and the gasified combustion products was carried out using process definitions for the reaction rate and the reaction velocity of chemical reactions. Subsequent to the chemical processes, the condensation process was considered as prozess in equilibrium state. The main product of the combustion of gasified aluminum and successive condensation is liquid aluminum oxide (Al_2O_3). Dependent on boundary conditions for relaxation in the nozzle also solid aluminium oxid, mostly as a glas phase, can be created.

Furthermore, in the paper the decomposition kinetics of alane (AlH_3), based on the limited available experimental data was defined. The short decomposition time indicate the very rapid process, which still takes place on the fuel surface or in its vicinity. As a decomposition product pure aluminum is generated, but only lasts for a split second. For this reason, alane particles were not further followed along the stream line.

In the future, the presented mathematical models will be extended to allow computations for other metals, metal alloys and metal hydrides such as Mg, Al-Mg alloy, MgH_2, etc.. CFD multiphase flow models provide, as shown here, a possibility to investigate the transformation kinetics of metal particles inside the combustion chamber of HRE and thus a better understanding of the entire process. This promising CFD tool will be further developed within the DLR ATEK research project. Within the project the numerical work will be supported by limited number of laboratory tests of various metal-containing fuel ingredients.

Abbreviations

ATEK	AntriebsTEchnologien für Kleinträger
CEA	Chemical Equilibrium with Applications
CFD	Computer Fluid Dynamic
HRE	Hybrid Rocket Engine
HTP	High Test Peroxide (H_2O_2 > 70%)
HTPB	Hydroxyl Terminated Polybutadiene
ODE	Ordinary Differential Equations

Important indices

chem	chemical
cloud	cloud volume (model)
con	convection
dec	decomposition
evap	evaporation
f	flame, reaction
gas	gas state
melt	melting
p	pressure
par	particle
rad	radiation
sol	solidification

References

[1] May, S., *Bestimmung der Wärmelasten am Düsenausgang eines Hybridraketentriebwerks.* Student research project, Institute of Aerospace Systems, Technical University Braunschweig and Institute of Aerodynamics and Flow Technology, German Aerospace Center (DLR), 2013.

[2] Božić, O., *Space Propulsion. Lecture Manuscript for Master Studies,* Technische Universität Braunschweig, 2014.

[3] Hartwig, A. *Metallhaltige Brennstoffe für Hybridraketentriebwerke.* Student research project *R 1023 S,* Institute of Aerospace Systems, Technical University Braunschweig and Institute of Aerodynamics and Flow Technology, German Aerospace Center (DLR), 2011.

[4] Weiser, V., Eisenreich, N., Koleczko, A., Roth, E. *On the Oxidation and Combustion of AlH_3 a Potential Fuel for Rocket Propellants and Gas Generators.* Propellants, Explosives and Pyrotechnics, 32: 213-221. WILEY-VCH Verlag GmbH Weinheim, 2007.

[5] Calabro, M. et al. *Advanced Hybrid Solid Fuels,* IAC-07-C4.2.09, 58th International Astronautical Congress, Hyderabad, 2007.

[6] Dupays, J. et al. *Combustion of Aluminium Particles in Solid Rocket Motors*, Proceedings ODAS 2000, 2nd ONERA – DLR Aerospace Symposium, 15th – 16th June 2000, Berlin (G)

[7] Escot Bocanegra, P. et al. *Studies on the Burning of Micro- and Nanoaluminium Particle Clouds in Air,* Progress in Propulsion Physics, Vol. 11. p. 47-62, EUCASS book series advances in aerospace sciences, Torus Press, 2009.

[8] Aly, Y. et al. *Reactive, Mechanically Alloyed Al-Mg Powders with Customized Particle Sizes and Compositions,* Journal of Propulsion and Power, 30(1): 96-104, New Jersey (USA), 2014.

[9] Selvaduray, G. *Binary Phase Diagrams. Presentation,* Materials Engineering Program, San Jose State University, San Jose.

[10] Bazyn, T. et al. *Combustion Characteristics of Aluminium Hydride at Elevated Pressure and Temperature.* Journal of Propulsion and Power, 20(3), pp. 427-431, May-June 2004.

[11] DeLuca, L.T. et al. *Ballistic Characterization of AlH_3-Based Propellants for Solid and Hybrid Rocket Propulsion. AIAA 2009-4874,* 45th AIAA/ASME/SAE/ASEE Joint Propulsion Conference & Exhibit, Denver (USA), 2009.

[12] DeLuca, L. T. et al. *Physical and Ballistic Characterization of AlH_3-based Space Propellants.* Aerospace Science and Technology, 11(1), pp.18-25, 2006.

[13] Funke, *Leichtmetallhydride als Raketentreibstoffe, Wissenschaftliche Veröffentlichung,* Wissenschaftliche Gesellschaft für Luft- und Raumfahrt, Frankfurt/Main, 1968.

[14] Bodak, O., Perrot, P. *Aluminium-Hydrogen-Lithium.* Light Metal Systems Part 3. Physical Chemistry IV, Landolt-Börnstein-Group, 2005.

[15] Grove, H., Løvvik, O. M., Huang, W., Opalka, S. M., Heyn, Richard H., Hauback, B. C., *Decomposition of Lithium Magnesium Aluminum Hydride.* Int. Journal of Hydrogene Energy, 36 (2011), pp. 7602-7611, ELSEVIER, May 2011.

[16] Werner, T. *Verbesserung der Wasserstoffspeicher-Eigenschaften eines reaktiven Hydridkomposites durch Optimierung des Herstellungsprozesses, Bachelorarbeit,* Hochschule für Angewandte Wissenschaften Hamburg, 2013.

[17] Sinke, G. C., Walker, L. C., Oetting, F.L., Stull, D. R., *Thermodynamic Properties of Aluminium Hydride,* The Journal of Chemical Physics, Vol. 47, No. 8, p. 2759, Michigan (USA), 1967.

[18] Antonov, V.E et al., *Heat Capacity of α-AlH_3 and α-AlD_3 at Temperatures up to 1000K,* J. Phys. Condens. Matter, 20(27): 275204, IOP Publishing, Moskva (Russia), 2008.

[19] Galfetti, L., DeLuca, L.T., Severini, F, Colombo, G., Meda, L., Marra, G. *Pre- and post-burning analysis of nano-aluminized solid rocket propellants,* Aerospace Science and Technology, 11, Jan. 2007, pp. 26-32 ELSEVIER

[20] Mokhtari Molk Abadi N., Transformation and Combustion Kinetics of Small Metal Particles within the Combustion Chamber of Hybrid Rocket Engines, Master thesis, Technical University Braunschweig and German Aerospace Center (DLR) – Institute of Aerodynamics and Flow Technology, Braunschweig, December 2014

[21] Puri, P., Yang, V. *Multi-Scale Modeling of Nano Aluminium Particle Ignition and Combustion,* In "Solid Propellant Chemistry, Combustion and Motor Interior Ballistics", p. 723-747, Editor-in-Chief: P. Zarchan, Vol. 185, Progress in Astronautics and Aeronautics, AIAA, Reston, Virginia, USA, 2000, ISBN 1-56347-422-5

[22] Beckstead, M.W., *A Summary of Aluminium Combustion, Paper RTO-EN-023,* RTO/VKI Special Course, Rhode-Saint-Genese (Belgium), 2002.

[23] Leithner, R. *Wärme- und Stoffübertragung, Vorlesungsskript,* Institut für Wärme- und Brennstofftechnik (IWBT), Technische Universität Braunschweig, 1996.

[24] Marxman, G. A., Wooldridge, C. E., Muzzy, R. J. *Fundamentals of Hybrid Boundary Layer Combustion. Paper* AIAA *63-505,* Palm Beach, Florida, 1963.

[25] Božić, O., *Numerical simulation of mineral transformation in the coal dust combustors,* Dissertation, Technische Universität Braunschweig , IWBT, Shaker Verlag, Aachen, Germany, 2003, ISBN 3-8322-1400-3

[26] May, S., Numerical Simulation of Flow and Combustion inside the Reaction Chamber of the AHRES Hybrid Rocket Engine, Master Thesis, German Aerospace Center (DLR), Braunschweig, Inst. Of Aerodynamics and Flow Technology, April 2014.

[27] Humble, R. W., Henry, G. N., Larson, W. J., *Space Propulsion Analysis and Design, Handbook,* McGraw-Hill Education, ISBN 978-0-07-723029-6 (2. release), 2007.

[28] Melcher, J.C., Burton, R. L., Krier, H., *Combustion of Aluminium Particles in Solid- Rocket Motor Flows,* AIAA Urbana (USA), in "Solid Propellant Chemistry Combustion, and Motor Interior Ballistics", p. 723-747, Editor-in-Chief: P. Zarchan, Vol. 185, Progress in Astronautics and Aeronautics, AIAA, Reston, Virginia, USA, 2000, ISBN 1-56347-422-5

[29] Gordon S., McBride B. J., NASA - GLENN Chemical Equilibrium Program CEA2, May 21, 2004, Refs: NASA RP-1311 (Part 1), 1994 and NASA RP-1311 (Part 2), 1996

[30] Gremyachkin V. M., Theory of Ignition of Metal Particles, Combustion, Explosion & Shock Waves, Vol. 22, No. 3, 1986, pp. 10-14